https://doi.org/10.5194/essd-2022-363
Preprint. Discussion started: 2 February 2023

Open Access Earth System Science Data Discussions

High-resolution digital elevation models and orthomosaics generated from historical aerial photographs (since the 1960s) of the Bale Mountains in Ethiopia

Mohammed Ahmed Muhammed[1, 2], Binyam Tesfaw Hailu[2, 3], Georg Miehe[4], Thomas Nauss[1], Dirk Zeuss[1]

[1]Department of Environmental Informatics, Faculty of Geography, Philipps-Universität Marburg, Deutschhausstraße 12, 35032, Marburg, Germany
[2]Remote Sensing and Geo-Informatics Stream, School of Earth Sciences, College of Natural and Computational Science, Addis Ababa University, Addis Ababa, 1176, Ethiopia,
[3]Department of Geosciences and Geography, University of Helsinki, PO Box 64 (Gustaf Hällströmin katu 2), FI-00014 Helsinki, Finland
[4]Department of Geography, Vegetation Geography, Philipps-Universität Marburg, Deutschhausstraße 10, 35032, Marburg, Germany

Correspondence to: Mohammed Ahmed (mohammed.muhammed@geo.uni-marburg.de, mohammed.ahmedgis@aau.edu.et)

Abstract. The natural resources of Ethiopian high-altitude ecosystems are commonly perceived as increasingly threatened by devastating land-use practices owing to decreasing lowland resources. Quantified time-series data of the course of land-use cover changes are still needed. Very high-resolution digital data on the historical landscape over the recent decades are needed for determining the impacts of changes in afro-alpine ecosystems. However, digital elevation models (DEMs) and orthomosaics do not exist for most afro-alpine ecosystems of Africa. We processed the only available and oldest historical aerial photographs for Ethiopia and, to the best of our knowledge, for any afro-alpine ecosystem. Here, we provide both DEM and orthomosaic images for the years 1967 and 1984 for the Bale Mountains in Ethiopia, which comprise the largest afro-alpine ecosystem in Africa. We used 298 historical aerial photographs captured in 1967 and 1984 for generating DEMs and orthomosaics with Structure from Motion Multi View Stereo Photogrammetry along an elevation gradient from 977 to 4377 m above sea level (asl) at spatial resolutions of 0.84 m and 0.98 m for the years 1967 and 1984, respectively. Our datasets can be used by researchers and policymakers for (1) watershed management, as the area provides water for more than 30 million people; (2) landscape management; (3) detailed mapping and analysis of geological and archaeological features, as well as natural resources; (4) analyses of geomorphological processes; and (5) biodiversity research.

https://doi.org/10.5194/essd-2022-363
Preprint. Discussion started: 2 February 2023

Open Access Earth System Science Data Discussions

1 Introduction

Landscapes worldwide are increasingly affected by anthropogenic and natural factors such as land use and climate change (Bendix et al., 2021; He et al., 2021; Huggel et al., 2012; Peters et al., 2019; Slaymaker and Embleton-Hamann, 2018). Afro-alpine ecosystems are particularly threatened due to population growth and human settlements, overgrazing, recurrent fire, deforestation, agricultural expansion (Gehrke and Linder, 2014; Gil-Romera et al., 2019; Kidane et al., 2012; Mezgebu and Workineh, 2017; Muhammed and Elias, 2021; Nyssen et al., 2014), and climate change (Colwell et al., 2008; Diaz and Bradley, 1997; Jacob et al., 2020; Kidane et al., 2022; Palomo, 2017). These impacts are of particular importance in afro-alpine ecosystems because they are hotspots of biodiversity and endemism (Gehrke and Linder, 2014; Merckx et al., 2015), and thus prominent for their ecological significance and considerable economic, recreational, aesthetic, and scientific value (Muhammed and Elias, 2021; Rahbek et al., 2019). They also constitute important freshwater sources for mountain and lowland ecosystems, as well as for millions of people living in the adjacent areas.

For analysing the effects of land use and climate change in afro-alpine ecosystems, digital data on the historical landscape at high spatial resolution are needed. Digital elevation models (DEMs) and orthomosaics are important data sources for quantifying the impacts of anthropogenic and natural changes. For instance, DEMs and orthomosaics can be used for research in structural geology (Da Costa and Starkey, 2001), earthquake impacts (Lu et al., 2021), archaeology (Risbøl et al., 2015), geomorphology (van Westen and Lulie Getahun, 2003), water resources management (Chignell et al., 2019), and land use land cover dynamics (Jacob et al., 2016). However, most studies have used satellite images with 10–60 m resolution (Kidane et al., 2012; Mezgebu and Workineh, 2017; Muhammed and Elias, 2021), freely available DEMs of 30 m or coarser resolution (Chignell et al., 2019; Farr et al., 2007; Friss et al., 2010; Kidane et al., 2022), and georeferenced aerial photographs with small spatial extent (< 225 km^2; Carta et al., 2018; Jacob et al., 2016; Johansson et al., 2019). However, no openly accessible historical DEMs and orthomosaics at high spatial resolution (< 5 m) and large spatial extent (> 127 km^2) exist for afro-alpine ecosystems. Currently, DEM and orthomosaics generated with unmanned aerial vehicles or helicopters reach spatial resolutions of 0.1 to 0.5 m with an extent ranging from 1.6 to 127 km^2 only in urban regions (Benoit et al., 2019; Bühler et al., 2012; Immerzeel et al., 2014).

In this study, we aim to present DEMs and orthomosaics for the years 1965/67 and 1984 at very high spatial resolutions (0.84 m and 0.98 m, respectively) for the remote Bale Mountains in Ethiopia, which comprise the largest afro-alpine ecosystem in Africa (Chignell et al., 2019). Our data can be used by researchers and policy makers for (1) watershed management, (2) analyses of historical landscape change, (3) detailed mapping and analyses of geological and archaeological features, as well as natural resources, (4) analyses of geomorphological processes, (5) socioecological patterns and dynamics, (6) modelling and planning for telecommunications, and (7) biodiversity research. Owing to its high spatial resolution and spatiotemporal coverage, our data will foster studies on the drivers of landscape change and its quantification.

https://doi.org/10.5194/essd-2022-363
Preprint. Discussion started: 2 February 2023

2 Material and Methods

2.1 Study area

The study area lies between 6º20′27″ to 7º51′17″ N and 39º16′58″ to 40º04′40″ E, (5730 km²) located 400 km southeast of Addis Ababa in the Oromia regional state of Ethiopia (Fig. 1). The area lies within the Bale Mountains and covers 25 % of the afro-alpine ecosystem of Africa (de Deus Vidal and Clark, 2020; Carbutt, 2020; Gehrke and Linder, 2014). The Bale Mountains were formed by lava outpourings of the Trappean series, which created a vast lava plateau considerably eroded and flattened by later glaciations (Berhe et al., 1987; Williams, 2017). The soils in the area tend to be shallow, gravelly, fertile silty loams of reddish-brown to black colour, as the parent rock is mainly basaltic and trachytic (Miehe and Miehe, 1994). The study area provides the water source for over 30 million people in Ethiopia, Somalia, and Kenya, and contributes to five major perennial rivers (Fig. 1).

The climate in the study area varies from north to south mainly owing to differences in elevation, aspect, and the influence of lowland hot air masses, which also influence the annual migration of the Intertropical Convergence Zone and Indian Ocean Monsoon (Miehe and Miehe, 1994). The mean monthly minimum and maximum temperatures are 5.6 °C and 21.4 °C, respectively, for an altitudinal range of 2700 to 4377 m above sea level (asl). The mean annual ground temperature ranges from 7 to 11 °C (Groos et al., 2022). The lowest and highest temperatures recorded on the Sanetti Plateau were -15 ºC and 26 ºC, respectively (Hillman, 1988), where frosts occur during all clear nights throughout the year (Groos et al., 2022). Rainfall is variable throughout the study area and ranges from 800 to 1500 mm annually (Woldu et al., 1989).

2.2 Data

We used historical aerial photographs (HAPs) taken in 1967 and 1984. They have a forward overlap of approximately 60 %, a side overlap of approximately 30 %, and were captured using an aerial 9 x 9-inch film frame camera, which was scanned at a resolution of 1200 dots per inch. The qualities of all scanned HAPs were excellent enough for processing with an image quality value above 0.5 units. For assessing the accuracy of our generated DEMs and orthomosaics, we used three sources of data: (1) Advanced Spaceborne Thermal Emission and Reflection Radiometer Global Digital Elevation Model (ASTER GDEM) data with a spatial resolution of 15 m, (2) data from the Shuttle Radar Topography Mission (SRTM) with a spatial resolution of 30 m, and (3) Advanced Land Observing Satellite Phased Array Type L band Synthetic Aperture Radar data (ALOS PALSAR) with a spatial resolution of 12.5 m. Each of the three downloaded DEMs were projected on the Adindan UTM coordinate system zone 37 N (EPSG: 20137) using ArcGIS Desktop version 10.8.2 (ESRI Inc., 2021).

https://doi.org/10.5194/essd-2022-363
Preprint. Discussion started: 2 February 2023

The 1967 HAPs were acquired by the United States Air Force under Project number AF 58-3, using a four-engine RC-130A aircraft flying at an altitude of 31,000 feet asl equipped with a KC-1(B) PLANIGON camera. For camera and lens number, calibrated focal length, magazine serial number, roll number, exact acquisition dates, and flight index map (see supplementary material (SM) Fig. S1 and Table S1). The shutter speed and aperture were 1/150 s and F-8, respectively, resulting in a scale of approximately 1:62,000.

The 1984 HAPs were obtained by SWEDSURVEY Company under project number "ET 1:5" using a Wild RC 10 camera (Wild Universal Aviogon II lens type, camera serial number 3045) with a calibrated focal length of 152.822 mm and a maximum aperture of F/4.0. The flight campaign had an average altitude of 7600 m asl and was conducted from 15–17 January, 1984. For more details on roll number, strip number, photo number, acquisition date, and flight index map see SM Fig. S2 and Table S2.

2.3 Data preparation

The data preparation step included extraction of the calibrated focal length, camera principal point coordinates, camera exposure stations, fiducial marks, and ground control points. All data preparation steps were performed with Agisoft Metashape Professional version 1.8.0.13794 (AgiSoft LLC, 2021), Google Earth, and ArcGIS Desktop version 10.8.2 (ESRI Inc., 2021).

2.3.1 Calibrated focal length

The calibrated focal length is a numerical best-balanced value used to determine the scale of the photograph. It is computed from the equivalent focal length to obtain minimum distortion and to match the lens distortion (Clarke and Fryer, 1998). The calibrated focal lengths were extracted from meta information on the HAPs of the film and from Spriggs (1966).

2.3.2 Principal points

A principal point is a point in the precise centre of a photograph. Its coordinates indicate the perpendicular interception of the optical axis of the lens with the sensor plane (SM Tables S5 and S6). Easting and Northing of the principal points (camera positions) were digitized from the scanned and georeferenced topographic flight index map, which included points of camera positions and polygons of consecutive aerial photograph coverage. Elevation data of the principal points were extracted using Google Earth. For the 1984 HAPs, the principal points were extracted from aero-triangulation documents in the Geospatial Information Institute of Ethiopia. For more details, see SM Tables S3 and S4.

2.3.3 Fiducial marks

Fiducial marks are markers rigidly connected to the centre or corners of the camera body. When the film is exposed, these marks appear on the film negative. Fiducial marks and their coordinates were used as input for the processing of scanned HAPs during the camera calibration workflow stage. For more details, see SM Figs. S3 and S4 along with Tables S5 and S6.

https://doi.org/10.5194/essd-2022-363
Preprint. Discussion started: 2 February 2023

125 **2.3.4 Ground control points**

Ground Control Points (GCPs) are locations on the ground localized by a spatial coordinate reference system. They were used to georeference the aerial camera data. We extracted 76 GCPs from Worldview-1 satellite imagery (Easting and Northing) accessed and downloaded from the database of the DFG research unit 2358 "The Mountain Exile Hypothesis" (http://vhrz669.hrz.uni-marburg.de/bale/) and Google Earth (elevation). These included 49 and 27 GCPs used to georefer-
130 ence the 1967 and the 1984 HAPs, respectively, as their acquisition and flight index differed. For more details, see SM Table S7.

3 Data processing

Data processing was performed using Structure-from-Motion Multi View Stereo Photogrammetry methodology by assigning appropriate values and settings in the main steps of loading the aerial photographs; aligning the cameras; building a dense
135 point cloud, mesh, digital elevation model, and orthomosaic; and exporting the results.

3.1 Structure-from-Motion Multi View Stereo Photogrammetry

Structure-from-Motion Multi View Stereo Photogrammetry (SfM MVS Photogrammetry) is applicable for soil erosion, volcanology, glaciology, coastal morphology, mass movements, and fluvial morphology. It was used in at least 65 scientific studies from 2012 to 2015 (Eltner et al., 2016) and also recently (Grottoli et al., 2020; Tomczyk and Ewertowski, 2021). The
140 advantages of SfM MVS Photogrammetry are that it can be applied fully automated (Eltner et al., 2016), is flexible, inexpensive, and requires little training (Westoby et al., 2012). The following steps were sequentially applied for generating DEMs and orthomosaics with SfM MVS Photogrammetry.

Aligning. This was the first step in the model generation process to generate tie points and match corresponding features using the Invariant Feature Transform algorithm (Lowe, 1999).

145 **Bundle adjustment.** Bundle adjustment was used for calculating individual camera positions and relative positions of corresponding features. A least-squares approach was used for estimating camera poses and 3D points.

Multi view stereo matching. Dense point clouds (multi view stereo) and 3D surfaces (build mesh) were calculated using known camera parameters (camera focal length, coordinates of the image principal point, lens distortion coefficients, omega, phi, and kappa) and with the SfM points as ground control. All pixels in all images were used, so the resulting dense model
150 was similar in resolution to the raw photographs.

Georectification. In this stage, the point cloud from an internal, arbitrary coordinate system was projected onto a geographical coordinate system. For the 1984 HAPs, the georectification process was completed using the camera positions and focal lengths, and for the 1967 HAPs by incorporating GCPs with known coordinates.

Derivative product generation. In this step, the final DEM and orthomosaics were created from the dense point clouds and
155 3D surfaces. For more details on the inputs and values used, see SM Table S9.

https://doi.org/10.5194/essd-2022-363
Preprint. Discussion started: 2 February 2023


Open Access Earth System Science Data Discussions

4 Results and discussion

The produced tie points resulted from the "align" step consisted of 412,903 (1967) and 450,071 (1984) filtered points, with low tie point reprojection errors ranging from 1.49 to 0.57 pixels, demonstrating the high quality of the image geometry network (Table 1). The dense point clouds consisted of 4,821,064,653 points for the 1967 HAPs and 6,501,301,603 points for the 1984 HAPs. These points were used to obtain a DEM and orthomosaic with spatial resolutions of 0.84 m and 0.98 m for 1967 and 1984 data, respectively (Figs. 2 and 3).

In a previous study, Frankl et al. (2015) processed 27 HAPs (both vertical and oblique) acquired in 1935 in the Suluh River Valley, Ethiopia, using SfM MVS and produced orthomosaics with planimetric and elevation root mean square error (RMSE) accuracy of 30 and 50.7 m, respectively. However, the accuracy of our DEMs produced for the years 1967 and 1984 was higher, with an RMSE of 3.55 and 3.44 m, respectively (Table 2). Considering that the SfM–MVS method yields accuracies of 1/1000 of the viewing distance, the elevations above the ground surface at which our HAPs were collected (8300 m for 1967 and 5068 m for 1984) yield acceptable error values of 8.3 and 5 m, respectively, which were achieved with our data products.

The orthomosaics and DEMs provided here will help to identify areas where changes in environmental characteristics occurred (e.g., encroachment of humans or deforestation of the Ericaceous vegetation in the north western part of the study area). For example, it became clear from our data that there was no severe human interference and deforestation before 1967. However, the 1984 orthomosaics provide evidence that people began intruding into Bale Mountains National Park and degraded the land by clearing vegetation near the settlements.

4.1 Example: quantification of volumetric change

Within the study area, soil material was excavated and used for constructing and repairing a gravel road (Fig. 4). An example volumetric analysis was done with Agisoft metashape professional software (AgiSoft LLC, 2021) for selected sites. The volumetric change calculated from the 1967 and 1984 DEMs was 14,728.9 m^3 for data example 1 (Fig. 4a, b) and 97,352 m^3 for data example 2 (Fig. 4e, f).

4.2 Quality assessment

The quality of the resulting dataset was assessed using external sources (509 GPS control points [CPs] collected in the field, as well as ASTER GDEM, SRTM DEM, and ALOS PALSAR points for both 1967 and 1984). Our generated DEMs have higher accuracies than previous DEMs (Fig. 5 and Table 2). As demonstrated by its RMSE value of 3.44, the DEM generated from the 1984 HAPs had the best quality. The 1967 DEM also had a very good quality, as indicated by an RMSE value of 3.55. The multiple R-squared value was 0.9998 (equal to the 1984 DEM) and there was no significant difference between 1967 and 1984 DEMs (Table 2).

https://doi.org/10.5194/essd-2022-363
Preprint. Discussion started: 2 February 2023

In addition, the resulting dataset was also assessed by internal precision as presented in Table 1. It indicates a high quality of internal image network geometry as huge dense point clouds for historical aerial photographs. This was illustrated by the low sub-pixel values of tie point reprojection errors of 1.49 and 0.68 pixels and the RMSE of 4.24 and 0.88 cm on the control points for the years 1967 and 1984, respectively. Among the three readily available DEMs used for the quality assessment, SRTM DEM had the highest quality (RMSE value of 5.64) in our study area, which has a complex topography and a huge elevation difference of 3800 m. These results agree with Sena et al. (2020). The SRTM DEM showed better precision (Fig. 5 and Table 2). However, others (Shebl and Csámer, 2021; Chowdhuri et al., 2021; Jalal et al., 2020) concluded that ALOS PALSAR is more accurate than the SRTM and ASTER DEMs and obtained different results for our study area. The ALOS PALSAR DEM (Fig. 5 and Table 2) was the next most accurate DEM with an RMSE vertical accuracy of 11.38. The ASTER GDEM was the least accurate in the area as the residual standard error value was 11.42 with an RMSE value of 11.54, indicating that there is a huge gap in elevation values compared to the field GPS control points (Fig. 5). Thomas et al. (2014) also attested to a higher accuracy for SRTM compared to ASTER.

5 Data availability

All described datasets are available in the Zenodo link repository https://doi.org/10.5281/zenodo.7271617 (Muhammed et al., 2022a) for the inputs and https://doi.org/10.5281/zenodo.7269999 (Muhammed et al., 2022b) for the results obtained. The structure of the dataset is as follows.

1 Unprocessed scanned aerial Photographs (approximately 36.1 GB) are available at https://doi.org/10.5281/zenodo.7271617 (Muhammed et al., 2022a). The images are zipped into four zipped folders named: "1967_Scanned_HAPs_Part1.7z" and "1967_Scanned_HAPs_Part2.7z" for the 1967 historical aerial photographs; and "1984_Scanned_HAPs_Part1.7z" and "1984_Scanned_HAPs_Part2.7z" for the 1984 historical aerial photographs. The scanned photographs are in Tiff format except four photographs in JPEG format.

2 Camera position coordinates (principal point coordinates) data are zipped into one folder "Camera_Position.zip" and two text files: "PP_1967.txt" and "PP_1984.txt" available at https://doi.org/10.5281/zenodo.7271617 (Muhammed et al., 2022a).

3 Flight index shapefile data are zipped into one folder named "Flight_Index.zip" with four shape files: "PP_1967.shp", "PP_1984.shp", "flight_index_1967.shp", and "flight_index_1984.shp"; and ground control point data are zipped into one folder named "GCP.zip" with two text files: "GCP_1967.txt" and "GCP_1984.txt available at https://doi.org/10.5281/zenodo.7271617 (Muhammed et al., 2022a).

4 The results of photogrammetric processing (approximately 32.5 GB) are available at https://doi.org/10.5281/zenodo.7269999 (Muhammed et al., 2022b), and are grouped into subfolders named: "DEM_1967.7z": inside the zipped folder "1967_DEM.tif" (digital elevation model for the year 1967), "DEM_1984.7z": inside the zipped folder "1984_DEM.tif" (digital elevation model for the year 1984), and

https://doi.org/10.5194/essd-2022-363
Preprint. Discussion started: 2 February 2023

"1967_Orthomosaic.7z" and "1984_Orthomosaic.7z" contain orthomosaic files "1967_orthomosaic.tif" and "1984_orthomosaic.tif" for the year 1967 and 1984, respectively. All data are in GeoTIFF format in the Adindan UTM Zone 37 N (EPSG: 20137) projected coordinate system.

Data extracted from the resulted study area for the volumetric calculation and visualization (approximately 1 MB) are available at https://doi.org/10.5281/zenodo.7269999 (Muhammed et al., 2022b) inside zipped folder "Data_Examples.Zip" and "Accuracy_assessment.7z" contains text and excel file used for accuracy assessment calculation. For more detail on the list of filenames for corresponding years and content descriptions, see SM Table S8.

6 Conclusions

We processed the only readily available and oldest historical aerial photographs for Ethiopia and, to the best of our knowledge, for any afro-alpine ecosystem. We generated the first historical high-resolution DEMs and orthomosaics for the years 1967 and 1984 at a larger spatial extent (5730 km^2) and a high spatial resolution (0.84 and 0.98 m, respectively). Our datasets will help the scientific community address various research questions related to the Bale Mountains and afro-alpine ecosystems in general.

Author contributions

MAM, BTH, GM, and TN created the research concept. MAM performed the photogrammetric processing and created the figures. MAM and GM conducted the field work. MAM and DZ drafted the manuscript, and MAM, DZ and BTH edited it. All authors contributed to the final version of the manuscript.

Competing interests

The authors declare that there are no conflicts of interest.

Acknowledgements

This research was funded by the German Research Council (DFG) in the framework of the joint Ethio-European Research Unit 2358 "The Mountain Exile Hypothesis: how humans benefited from and re-shaped African high-altitude ecosystems during Quaternary climatic changes".

We thank the Geospatial Information Institute of Ethiopia for provided us the necessary data and documents; and Ethiopian Wildlife Conservation Authority, the Philipps University of Marburg, the Ethiopian Wolf Project, and the Bale Mountains National Park for their cooperation and permission to conduct field work. We also very much appreciate the support of Mohammed Kedir, Hussein, Gash Kasim, Awol Assefa, Sofia, Wege Abebe, and Katinka Thielsen, without whom it would not

have been possible to do the field work in the Bale Mountains. We thank Spaska Forteva for her help in arranging lab facilities. We also would like to acknowledge the anonymous reviewers.

Financial support

This work was supported by Deutsche Forschung gemeinschaft (DFG) Award no. **NA 783/12-1, AOBJ 628803** through a project entitled "The mountain exile hypothesis: how humans benefited from and re-shaped African high-altitude ecosystems during Quaternary climatic changes" within the framework of Research Unit 2358.

References

AgiSoft LLC: Agisoft Metashape Professional, 2021.

Bendix, J., Aguire, N., Beck, E., Bräuning, A., Brandl, R., Breuer, L., Böhning-Gaese, K., de Paula, M. D., Hickler, T., Homeier, J., Inclan, D., Leuschner, C., Neuschulz, E. L., Schleuning, M., Suarez, J. P., Trachte, K., Wilcke, W., Windhorst, D., and Farwig, N.: A research framework for projecting ecosystem change in highly diverse tropical mountain ecosystems, Oecologia, 195, 589–600, https://doi.org/10.1007/s00442-021-04852-8, 2021.

Benoit, L., Gourdon, A., Vallat, R., Irarrazaval, I., Gravey, M., Lehmann, B., Prasicek, G., Gräff, D., Herman, F., and Mariethoz, G.: A high-resolution image time series of the Gorner Glacier – Swiss Alps – derived from repeated unmanned aerial vehicle surveys, Earth Syst. Sci. Data, 11, 579–588, https://doi.org/10.5194/essd-11-579-2019, 2019.

Berhe, S. M., Desta, B., Nicoletti, M., and Teferra, M.: Geology, geochronology and geodynamic implications of the Cenozoic magmatic province in W and SE Ethiopia, J. Geol. Soc., 144, 213–226, https://doi.org/10.1144/gsjgs.144.2.0213, 1987.

Bühler, Y., Marty, M., and Ginzler, C.: High resolution DEM generation in high-alpine terrain using airborne remote sensing techniques: high resolution DEM generation in high-alpine terrain, T. GIS, 16, 635–647, https://doi.org/10.1111/j.1467-9671.2012.01331.x, 2012.

Carbutt, C.: Nature of alpine ecosystems in tropical mountains of Africa, in: Enc. World's Biomes, Els., 292–299, https://doi.org/10.1016/B978-0-12-409548-9.11753-1, 2020.

Carta, A., Taboada, T., and Müller, J. V.: Diachronic analysis using aerial photographs across fifty years reveals significant land use and vegetation changes on a Mediterranean island, Appl. Geogr., 98, 78–86, https://doi.org/10.1016/j.apgeog.2018.07.010, 2018.

Chignell, S. M., Laituri, M. J., Young, N. E., and Evangelista, P. H.: Afroalpine wetlands of the Bale Mountains, Ethiopia: Distribution, dynamics, and conceptual Flow Model, Ann. Am. Assoc. Geogr., 109, 791–811, https://doi.org/10.1080/24694452.2018.1500439, 2019.

Chowdhuri, I., Pal, S. C., Saha, A., Chakrabortty, R., and Roy, P.: Evaluation of different DEMs for gully erosion susceptibility mapping using in-situ field measurement and validation, Ecol. Inform., 65, 101425, https://doi.org/10.1016/j.ecoinf.2021.101425, 2021.

Clarke, T. A. and Fryer, J. G.: The development of camera calibration methods and models, Photogramm. Rec., 16, 51–66, https://doi.org/10.1111/0031-868X.00113, 1998.

Colwell, R. K., Brehm, G., Cardelús, C. L., Gilman, A. C., and Longino, J. T.: Global Warming, Elevational Range Shifts, and Lowland Biotic Attrition in the Wet Tropics, Science, 322, 258–261, https://doi.org/10.1126/science.1162547, 2008.

da Costa, R. D., and Starkey, J.: PhotoLin: A program to identify and analyze linear structures in aerial photographs, satellite images and maps, Comput. Geosci., 27, 527–534, https://doi.org/10.1016/S0098-3004(00)00146-1, 2001.

de Deus, Vidal J., and Clark, V. R.: Afro-alpine plant diversity in the tropical mountains of Africa, in: Enc. World's Biomes, Els., 373–394, https://doi.org/10.1016/B978-0-12-409548-9.11885-8, 2020.

Diaz, H. F. and Bradley, R. S.: Temperature Variations During the Last Century at High Elevation Sites, in: Climatic Change at High Elevation Sites, edited by: Diaz, H. F., Beniston, M., and Bradley, R. S., Springer Netherlands, Dordrecht, 21–47, https://doi.org/10.1007/978-94-015-8905-5_2, 1997.

Eltner, A., Kaiser, A., Castillo, C., Rock, G., Neugirg, F., and Abellán, A.: Image-based surface reconstruction in geomorphometry – merits, limits and developments, Earth Surf. Dynam., 4, 359–389, https://doi.org/10.5194/esurf-4-359-2016, 2016.

ESRI Inc.: ArcGIS Desktop, 2021.

Farr, T. G., Rosen, P. A., Caro, E., Crippen, R., Duren, R., Hensley, S., Kobrick, M., Paller, M., Rodriguez, E., Roth, L., Seal, D., Shaffer, S., Shimada, J., Umland, J., Werner, M., Oskin, M., Burbank, D., and Alsdorf, D.: The shuttle radar topography mission, Rev .Geophys., 45, RG2004, https://doi.org/10.1029/2005RG000183, 2007.

Friss, I., Demissew, S., and van Breugel, P.: Atlas of the potential vegetation of Ethiopia, Det Kongelige Danske Videnskabernes Selskab, Copenhagen, Denmark, 307 pp, 2010.

https://doi.org/10.5194/essd-2022-363
Preprint. Discussion started: 2 February 2023

Gehrke, B. and Linder, H. P.: Species richness, endemism and species composition in the tropical Afroalpine flora, Alp. Bot., 124, 165–177, https://doi.org/10.1007/s00035-014-0132-0, 2014.

Gil-Romera, G., Adolf, C., Benito, B. M., Bittner, L., Johansson, M. U., Grady, D. A., Lamb, H. F., Lemma, B., Fekadu, M., Glaser, B., Mekonnen, B., Sevilla-Callejo, M., Zech, M., Zech, W., and Miehe, G.: Long-term fire resilience of the Ericaceous Belt, Bale Mountains, Ethiopia, Biol. Lett., 15, 20190357, https://doi.org/10.1098/rsbl.2019.0357, 2019.

Groos, A. R., Niederhauser, J., Lemma, B., Fekadu, M., Zech, W., Hänsel, F., Wraase, L., Akçar, N., and Veit, H.: An hourly ground temperature dataset for 16 high-elevation sites (3493–4377 m a.s.l.) in the Bale Mountains, Ethiopia (2017–2020), Earth Syst. Sci. Data, 14, 1043–1062, https://doi.org/10.5194/essd-14-1043-2022, 2022.

Grottoli, E., Biausque, M., Rogers, D., Jackson, D. W. T., and Cooper, J. A. G.: Structure-from-motion-derived digital surface models from historical aerial photographs: A New 3D Application for Coastal Dune Monitoring, Remote Sensing, 13, 95, https://doi.org/10.3390/rs13010095, 2020.

He, G., Zhao, X., and Yu, M.: Exploring the multiple disturbances of karst landscape in Guilin World Heritage Site, China, CATENA, 203, 105349, https://doi.org/10.1016/j.catena.2021.105349, 2021.

Hillman, J. C.: The Bale Mountains national park area, Southeast Ethiopia, and its management, Mt. Res. Dev., 8, 253, https://doi.org/10.2307/3673456, 1988.

Huggel, C., Clague, J. J., and Korup, O.: Is climate change responsible for changing landslide activity in high mountains?: CLIMATE CHANGE AND LANDSLIDES IN HIGH MOUNTAINS, Earth Surf. Proc. Landf., 37, 77–91, https://doi.org/10.1002/esp.2223, 2012.

Immerzeel, W. W., Kraaijenbrink, P. D. A., Shea, J. M., Shrestha, A. B., Pellicciotti, F., Bierkens, M. F. P., and de Jong, S. M.: High-resolution monitoring of Himalayan glacier dynamics using unmanned aerial vehicles, Remote Sens. Environ., 150, 93–103, https://doi.org/10.1016/j.rse.2014.04.025, 2014.

Jacob, M., Romeyns, L., Frankl, A., Asfaha, T., Beeckman, H., and Nyssen, J.: Land use and cover dynamics since 1964 in the Afro-alpine vegetation belt: Lib Amba Mountain in North Ethiopia, Land Degrad. Dev., 27, 641–653, https://doi.org/10.1002/ldr.2396, 2016.

Jacob, M., De Ridder, M., Vandenabeele, M., Asfaha, T., Nyssen, J., and Beeckman, H.: The Response of Erica arborea L. Tree Growth to Climate Variability at the Afro-alpine Tropical Highlands of North Ethiopia, Forests, 11, 310, https://doi.org/10.3390/f11030310, 2020.

Jalal, S. J., Musa, T. A., Ameen, T. H., Din, A. H. M., Aris, W. A. W., and Ebrahim, J. M.: Optimizing the Global Digital Elevation Models (GDEMs) and accuracy of derived DEMs from GPS points for Iraq's mountainous areas, Geodesy and Geodynamics, 11, 338–349, https://doi.org/10.1016/j.geog.2020.06.004, 2020.

Johansson, M. U., Senay, S. D., Creathorn, E., Kassa, H., and Hylander, K.: Change in heathland fire sizes inside vs. outside the Bale Mountains National Park, Ethiopia, over 50 years of fire-exclusion policy: lessons for REDD+, E&S, 24, art26, https://doi.org/10.5751/ES-11260-240426, 2019.

Kidane, Y., Stahlmann, R., and Beierkuhnlein, C.: Vegetation dynamics, and land use and land cover change in the Bale Mountains, Ethiopia, Environ. Monit. Assess., 184, 7473–7489, https://doi.org/10.1007/s10661-011-2514-8, 2012.

Kidane, Y. O., Hoffmann, S., Jaeschke, A., Beloiu, M., and Beierkuhnlein, C.: Ericaceous vegetation of the Bale Mountains of Ethiopia will prevail in the face of climate change, Sci. Rep., 12, 1858, https://doi.org/10.1038/s41598-022-05846-z, 2022.

Lowe, D. G.: Object recognition from local scale-invariant features, in: Proceedings of the Seventh IEEE International Conference on Computer Vision, Proceedings of the Seventh IEEE International Conference on Computer Vision, Kerkyra, Greece, 1150–1157 vol.2, https://doi.org/10.1109/ICCV.1999.790410, 1999.

Lu, L., Zhou, Y., and Walker, R. T.: Using historical aerial photographs to measure earthquake deformation: Testing the effects of scan resolution, Remote Sens. Environ., 252, 112118, https://doi.org/10.1016/j.rse.2020.112118, 2021.

Merckx, V. S. F. T., Hendriks, K. P., Beentjes, K. K., Mennes, C. B., Becking, L. E., Peijnenburg, K. T. C. A., Afendy, A., Arumugam, N., de Boer, H., Biun, A., Buang, M. M., Chen, P.-P., Chung, A. Y. C., Dow, R., Feijen, F. A. A., Feijen, H., Soest, C. F., Geml, J., Geurts, R., Gravendeel, B., Hovenkamp, P., Imbun, P., Ipor, I., Janssens, S. B., Jocqué, M., Kappes, H., Khoo, E., Koomen, P., Lens, F., Majapun, R. J., Morgado, L. N., Neupane, S., Nieser, N., Pereira, J. T., Rahman, H., Sabran, S., Sawang, A., Schwallier, R. M., Shim, P.-S., Smit, H., Sol, N., Spait, M., Stech, M., Stokvis, F., Sugau, J. B., Sulei-man, M., Sumail, S., Thomas, D. C., van Tol, J., Tuh, F. Y. Y., Yahya, B. E., Nais, J., Repin, R., Lakim, M., and Schilthuizen, M.: Evolution of endemism on a young tropical mountain, Nature, 524, 347–350, https://doi.org/10.1038/nature14949, 2015.

Mezgebu, A. and Workineh, G.: Changes and drivers of afro-alpine forest ecosystem: future trajectories and management strategies in Bale eco-region, Ethiopia, Ecol. Process, 6, 42, https://doi.org/10.1186/s13717-017-0108-2, 2017.

Miehe, S. and Miehe, G.: Ericaceous Forests and Heathlands in the Bale Mountains of South Ethiopia Ecology and Man's Impact, Traute Warnke Verlag, Reinbek, Hamburg, Germany, 161 pp., 1994.

https://doi.org/10.5194/essd-2022-363
Preprint. Discussion started: 2 February 2023

Muhammed, A., and Elias, E.: The effects of landscape change on plant diversity and structure in the Bale Mountains National Park, Southeastern Ethiopia, Int. J. Ecol., 2021, 1–13, https://doi.org/10.1155/2021/6628282, 2021.

Muhammed, M. A., Hailu, B. T., Miehe, G., Nauss, T., Zeuss, D.: High-resolution digital elevation models and orthomosaics generated from historical aerial photographs (since the 1960s) of the Bale Mountains in Ethiopia, Zenodo [data set], https://doi.org/10.5281/zenodo.7271617, 2022a.

Muhammed, M. A., Hailu, B. T., Miehe, G., Nauss, T., Zeuss, D.: High-resolution digital elevation models and orthomosaics generated from historical aerial photographs (since the 1960s) of the Bale Mountains in Ethiopia, Zenodo [data set], https://doi.org/10.5281/zenodo.7269999, 2022b.

Nyssen, J., Frankl, A., Haile, M., Hurni, H., Descheemaeker, K., Crummey, D., Ritler, A., Portner, B., Nievergelt, B., Moeyersons, J., Munro, N., Deckers, J., Billi, P., and Poesen, J.: Environmental conditions and human drivers for changes to north Ethiopian mountain landscapes over 145 years, Sci. Total Environ., 485–486, 164–179, https://doi.org/10.1016/j.scitotenv.2014.03.052, 2014.

Palomo, I.: Climate Change Impacts on Ecosystem Services in High Mountain Areas: A Literature Review, Mt. Res. Dev., 37, 179–187, https://doi.org/10.1659/MRD-JOURNAL-D-16-00110.1, 2017.

Peters, M. K., Hemp, A., Appelhans, T., Becker, J. N., Behler, C., Classen, A., Detsch, F., Ensslin, A., Ferger, S. W., Frederiksen, S. B., Gebert, F., Gerschlauer, F., Gütlein, A., Helbig-Bonitz, M., Hemp, C., Kindeketa, W. J., Kühnel, A., Mayr, A. V., Mwangomo, E., Ngereza, C., Njovu, H. K., Otte, I., Pabst, H., Renner, M., Röder, J., Rutten, G., Schellenberger Costa, D., Sierra-Cornejo, N., Vollstädt, M. G. R., Dulle, H. I., Eardley, C. D., Howell, K. M., Keller, A., Peters, R. S., Ssymank, A., Kakengi, V., Zhang, J., Bogner, C., Böhning-Gaese, K., Brandl, R., Hertel, D., Huwe, B., Kiese, R., Kleyer, M., Kuzyakov, Y., Nauss, T., Schleuning, M., Tschapka, M., Fischer, M., and Steffan-Dewenter, I.: Climate–land-use interactions shape tropical mountain biodiversity and ecosystem functions, Nature, 568, 88–92, https://doi.org/10.1038/s41586-019-1048-z, 2019.

Rahbek, C., Borregaard, M. K., Colwell, R. K., Dalsgaard, B., Holt, B. G., Morueta-Holme, N., Nogues-Bravo, D., Whittaker, R. J., and Fjeldså, J.: Humboldt's enigma: What causes global patterns of mountain biodiversity?, Science, 365, 1108–1113, https://doi.org/10.1126/science.aax0149, 2019.

Risbøl, O., Briese, C., Doneus, M., and Nesbakken, A.: Monitoring cultural heritage by comparing DEMs derived from historical aerial photographs and airborne laser scanning, J. Cult. Herit., 16, 202–209, https://doi.org/10.1016/j.culher.2014.04.002, 2015.

Sena, N. C., Veloso, G. V., Fernandes-Filho, E. I., Francelino, M. R., and Schaefer, C. E. G. R.: Analysis of terrain attributes in different spatial resolutions for digital soil mapping application in south eastern Brazil, Geoderma. Reg., 21, e00268, https://doi.org/10.1016/j.geodrs.2020.e00268, 2020.

Shebl, A., and Csámer, Á.: Reappraisal of DEMs, Radar and optical datasets in lineaments extraction with emphasis on the spatial context, Remote Sensing Applications: Society and Environment, 24, 100617, https://doi.org/10.1016/j.rsase.2021.100617, 2021.

Slaymaker, O. and Embleton-Hamann, C.: Advances in global mountain geomorphology, Geomorphology, 308, 230–264, https://doi.org/10.1016/j.geomorph.2018.02.016, 2018.

Spriggs, R. M.: The Calibration of Military Cartography Cameras, https://archive.org/, 1966.

Thomas, J., Joseph, S., Thrivikramji, K. P., and Arunkumar, K. S.: Sensitivity of digital elevation models: The scenario from two tropical mountain river basins of the Western Ghats, India, Geosci. Front., 5, 893–909, https://doi.org/10.1016/j.gsf.2013.12.008, 2014.

Tomczyk, A. M., and Ewertowski, M. W.: Baseline data for monitoring geomorphological effects of glacier lake outburst flood: a very-high-resolution image and GIS datasets of the distal part of the Zackenberg River, northeast Greenland, Earth Syst. Sci. Data, 13, 5293–5309, https://doi.org/10.5194/essd-13-5293-2021, 2021.

van Westen, C. J., and Lulie Getahun, F.: Analyzing the evolution of the Tessina landslide using aerial photographs and digital elevation models, Geomorphology, 54, 77–89, https://doi.org/10.1016/S0169-555X(03)00057-6, 2003.

Westoby, M. J., Brasington, J., Glasser, N. F., Hambrey, M. J., and Reynolds, J. M.: 'Structure-from-Motion' photogrammetry: A low-cost, effective tool for geoscience applications, Geomorphology, 179, 300–314, https://doi.org/10.1016/j.geomorph.2012.08.021, 2012.

Williams, P. W.: Glaciations and Climate Change, in: New Zealand Landscape, Els, 301–335, https://doi.org/10.1016/B978-0-12-812493-2.00007-4, 2017.

Woldu, Z., Feoli, E., and Nigatu, L.: Partitioning an elevation gradient of vegetation from south eastern Ethiopia by probabilistic methods, Vegetatio, 81, 189–198, https://doi.org/10.1007/BF00045524, 1989.

https://doi.org/10.5194/essd-2022-363
Preprint. Discussion started: 2 February 2023

Figures and Tables

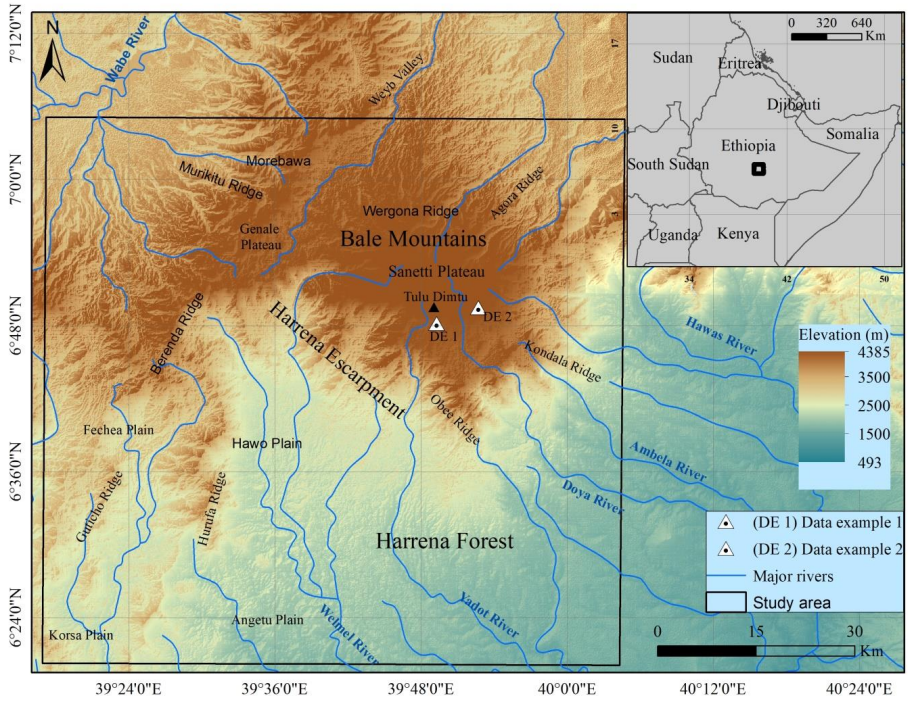

Figure 1. Study area in the southern Ethiopian highlands, east Africa. Data: Shuttle Radar Thematic Mapper (United States Geological Survey), Ethio-GIS (Central Statistics Agency)

https://doi.org/10.5194/essd-2022-363
Preprint. Discussion started: 2 February 2023

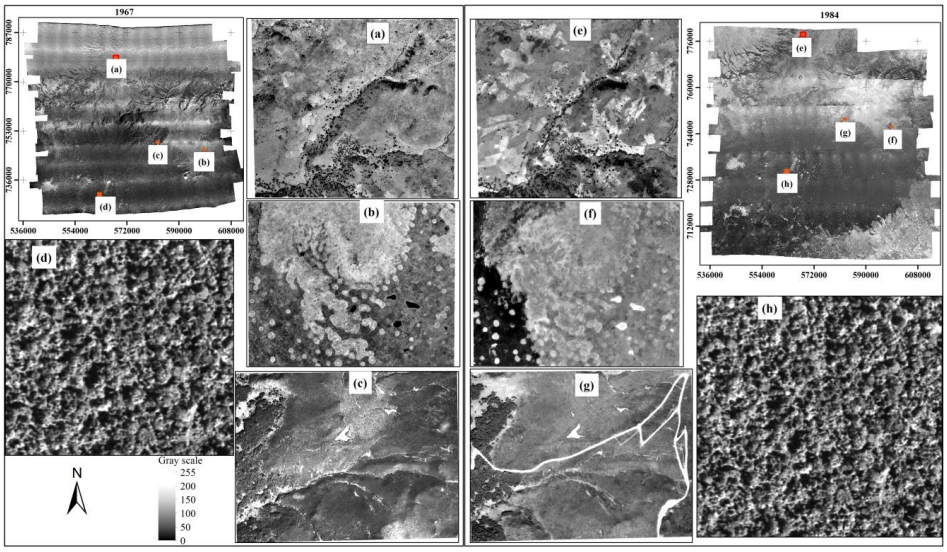

Figure 2. Orthomosaics generated for 1967 (a–d) and 1984 (e–h) showing encroachment and cultivation of land in the north western portion of the study area, (a) and (e); forested area, (d) and (h); wetland area with earth mounds of ground-dwelling small mammals, (b) and (f); gravel road construction in 1984, (g); and no visible road constructed in 1967, (c)

https://doi.org/10.5194/essd-2022-363
Preprint. Discussion started: 2 February 2023

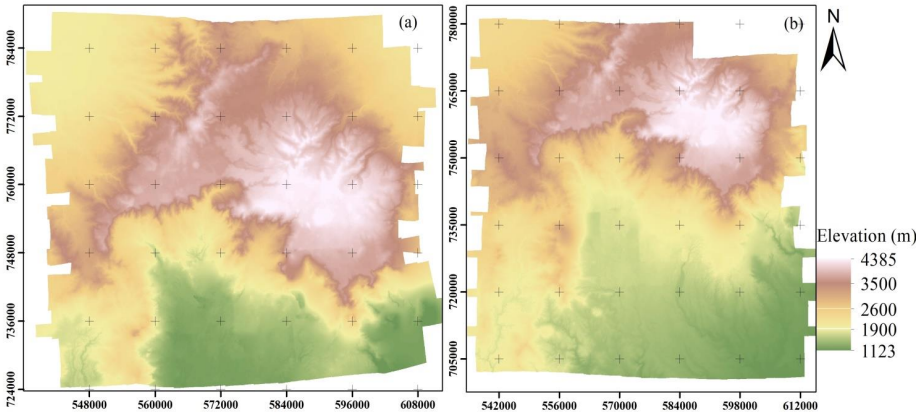

Figure 3. Digital elevation models generated for the afro-alpine ecosystem of the Bale mountains in Ethiopia from scanned historical aerial photographs for the years 1967 (a) and 1984 (b)

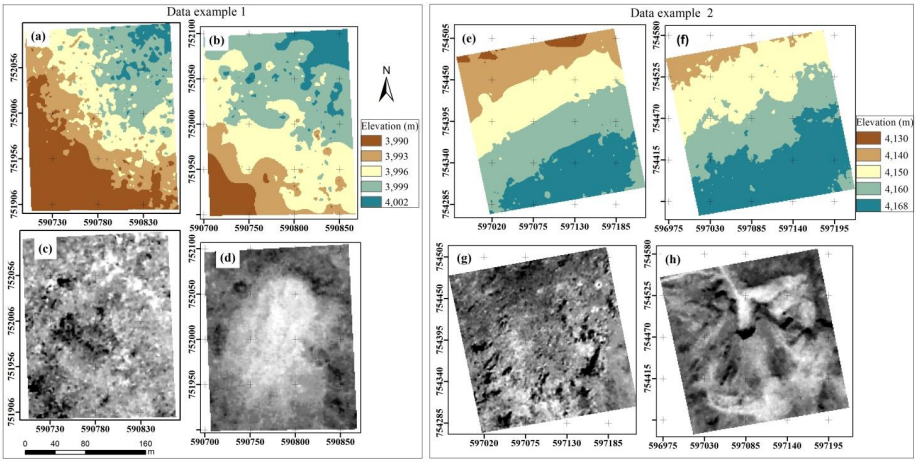

Figure 4. Digital elevation model extent used for calculating the volumetric change in the study area for two example sites between the years 1967 and 1984: (a), (b), (e), and (f) for data examples 1 and 2 (see Fig. 1). Orthomosaics showing the planimetric extent of the extracted selected material: (c), (d), (g), and (h) at the centre of the study area, the Sanetti plateau. The 1967 orthomosaics (c) and (g) depict no excavation. The1984 orthomosaics (d) and (h) show the excavation and gravel road construction to Delo Menna town (toward the southeast) and Goba town (towards the north). See also Fig. 1.

https://doi.org/10.5194/essd-2022-363
Preprint. Discussion started: 2 February 2023

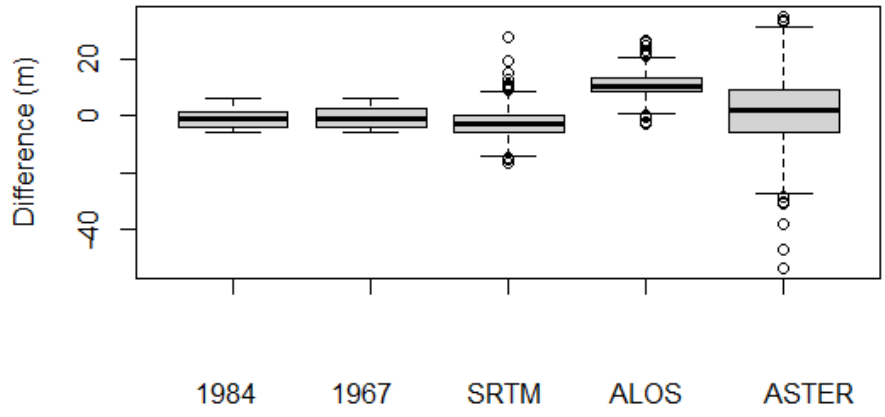

Figure 5. Comparison of the distribution of error in elevation value differences between each GPS control point collected in the field and the DEMs generated for the years 1984 and 1967, and the readily available DEMs: ALOS PALSAR, SRTM, and ASTER

https://doi.org/10.5194/essd-2022-363
Preprint. Discussion started: 2 February 2023

Open Access Earth System Science Data Discussions

Table 1. Parameters, processing errors, and final product characteristics used and obtained in this study

	Acquisition year	
	1965/67	1984
Camera model	KC-1B	WILD RC 10
Image size (pixels)	12,000 x 12,000	12,000 x 12,000
Focal length (mm)	default	152.822
Pixel size (μm)	20	20
Camera shutter type	Mechanical	Mechanical
Coverage (km^2)	4370	5730
Average flight height asl (m)	9448	7600
Number of images	145	153
Ground sampling distance (m/pix)	0.84	0.98
Number of tie points after filtration	412,903	450,071
Number of dense point clouds	4,821,064,653	6,501,301,603
Tie point RMS reprojection error (pix)	1.49	0.68
Average tie point multiplicity	2.19	2.26
Mean key point size	4.90	4.75
Dense cloud point density (point m^{-2})	1.41	1.03
Number of control points	49	27
Total (3D) RMSE (cm) on control points	4.24	0.88

https://doi.org/10.5194/essd-2022-363
Preprint. Discussion started: 2 February 2023

Open Access Earth System Science Data Discussions

Table 2. Quality assessment showing statistical differences between control points and the respective points in the five DEMs (Min = minimum elevation difference from field control points, 1Q = first quantile, Med = median, 3Q = third quantile; Max = maximum elevation difference from control points, RSE = Residual Standard Error, M R^2 = Multiple R-Squared, and RMSE = Root Mean Square Error)

Data	Min	1Q	Med	3Q	Max	RSE	M R^2	RMSE
CP- 1984	-5.56	-2.79	-0.04	2.41	7.40	3.22	0.9998	3.44
CP- 1967	-5.84	-2.88	-0.12	2.94	7.73	3.41	0.9998	3.55
CP- ALOS PALSAR	-12.47	-2.62	-0.21	2.39	14.82	4.05	0.9997	11.38
CP- SRTM	-14.03	-2.92	-0.49	2.71	29.95	4.87	0.9995	5.64
CP- ASTER	-54.58	-7.76	-0.05	7.25	32.40	11.42	0.9974	11.54